ADVANCED HEALTHCARE MATERIALS
www.advhealthmat.de

Light Weight and Flexible High-Performance Diagnostic Platform

Daniil Karnaushenko, Bergoi Ibarlucea, Sanghun Lee, Gungun Lin, Larysa Baraban, Sebastian Pregl, Michael Melzer, Denys Makarov,* Walter M. Weber, Thomas Mikolajick, Oliver G. Schmidt, and Gianaurelio Cuniberti*

A flexible diagnostic platform is realized and its performance is demonstrated for early detection of avian influenza virus (AIV) subtype H1N1 DNA sequences. The key component of the platform is high-performance biosensors based on high output currents and low power dissipation Si nanowire field effect transistors (SiNW-FETs) fabricated on flexible 100 µm thick polyimide foils. The devices on a polymeric support are about ten times lighter compared to their rigid counterparts on Si wafers and can be prepared on large areas. While the latter potentially allows reducing the fabrication costs per device, the former makes them cost efficient for high-volume delivery to medical institutions in, e.g., developing countries. The flexible devices withstand bending down to a 7.5 mm radius and do not degrade in performance even after 1000 consecutive bending cycles. In addition to these remarkable mechanical properties, on the analytic side, the diagnostic platform allows fast detection of specific DNA sequences of AIV subtype H1N1 with a limit of detection of 40×10^{-12} M within 30 min suggesting its suitability for early stage disease diagnosis.

1. Introduction

The development of modern multifunctional biomedical devices for health monitoring, point-of-care diagnostics, and environmental sensing has attracted extensive interest in the last two decades.[1–4] However, the world-wide deployment of some of these devices is hampered by their potentially high cost that is not readily affordable for, e.g., developing countries. In particular, high risks of an epidemic spread of severe diseases under resource-limited conditions require timely diagnosis so that early treatment can be made.[5–7] Not least facing the current west African Ebola thread, one of the major strategies outlined by the World Health Organization (WHO) in the recently published report[8] is to support interdisciplinary researches, which would enable novel methods for more efficient and precise detection and treatment of the pathogens such as seasonal, pandemic, and zoonotic influenza viruses in order to boost the level of achievements in modern medicine.

Depending on the detected species, the diagnostic devices should provide sensitivity to biochemical species at concentrations in the pM–nM range. In this way, successful early stage diagnoses of manifold diseases can be assured as needed, for instance for preventing the spread of influenza viruses.[9] Since most of the bioanalysis tools are realized at the surface, i.e., ELISA or microarrays, high sensitivities can be achieved using functional elements with extremely high surface-to-volume ratio. The latter is a unique property distinguishing biosensors based on Si nanowire field effect transistors (SiNW-FETs),[10–12]

D. Karnaushenko, G. Lin, M. Melzer, Dr. D. Makarov, Prof. O. G. Schmidt
Institute for Integrative Nanosciences
IFW Dresden
Helmholtzstr. 20, 01069 Dresden, Germany
E-mail: d.makarov@ifw-dresden.de

Dr. B. Ibarlucea, S. Lee, Dr. L. Baraban, S. Pregl, Prof. G. Cuniberti
Institute for Materials Science and
Max Bergmann Center of Biomaterials
Dresden University of Technology
Budapesterstr. 27, 01062 Dresden, Germany
E-mail: larysa.baraban@nano.tu-dresden.de

Dr. B. Ibarlucea, S. Pregl, Dr. W. M. Weber, Prof. T. Mikolajick, Prof. O. G. Schmidt, Prof. G. Cuniberti
Center for Advancing Electronics Dresden (CfAED)
Dresden University of Technology
01062 Dresden Germany

S. Pregl, Dr. W. M. Weber, Prof. T. Mikolajick
Namlab GmbH
Nöthnitzerstraße 64, 01187 Dresden, Germany

Prof. T. Mikolajick
Institute for Semiconductors and Microsystems
Dresden University of Technology
01062 Dresden, Germany

Prof. O. G. Schmidt
Material Systemsfor Nanoelectronics
Chemnitz University of Technology
Reichenhainer Str. 70, 09107 Chemnitz, Germany

Prof. G. Cuniberti
Dresden Center for Computational Materials Science (DCCMS)
Dresden University of Technology
01062 Dresden, Germany

DOI: 10.1002/adhm.201500128

which are already proven to be successful in detecting biochemical species down to the single molecule level.[13,14] Si nanowires are easily modifiable with organic and inorganic functional groups[15–17] enabling selective sensitivity to particular bio- and chemical substances of interest, e.g., molecules, viruses, antibodies, cells. These features, accompanied with a high power efficiency, enable the use of SiNW-FETs as biochemical sensors for point-of-care, rapid diagnostics, and personal safety.[18]

To bring state-of-the-art biomedical diagnostic devices to the hands of the people in need, a primary task is to reduce the price of the devices and allow for their high-volume delivery in a cost-efficient manner, e.g., container transportation.[19] For the latter, a crucial aspect is to reduce the weight of the device. This can be achieved by replacing the conventional rigid substrates, like Si or glass by light weight and large area polymeric foils.[20,21] To this end, flexible diagnostic or analytic devices on paper,[22] textile,[23] or polymers[24,25] have been demonstrated to address the emerging needs of low cost and ultralight weight of the biosensing platforms. Various flexible devices have been realized as components for smart medical implants,[26,27] epidermal electronics,[28] as well as the electronic skins,[21,29] which already allow to perceive temperature changes,[30] monitor and display physiological conditions,[28] perceive the presence of magnetic fields,[31–33] and communicate wirelessly and harvest and store energy for autonomous operation.[34,35]

Here, we realized a flexible light weight diagnostic platform based on SiNW-FETs revealing remarkable limit of detection at 40×10^{-12} M for avian influenza virus (AIV) subtype H1N1 DNA sequences. The H1N1 subtype of AIV was chosen as it is considered a global major risk for human health, exemplified by the declaration as pandemic to the 2009 swine-origin one.[36] A strong advantage of the developed platform on lightweight 100 µm thick flexible foils over conventional electronics fabricated on rigid substrates is the possibility of fabrication over large areas (**Figure 1**) and adaptivity by redesigning the final product on demand. For instance, a single working unit on a flexible foil can be cut out (Movie S1, Supporting Information), or redundant parts of the support for specific applications can be removed simply by cutting. Furthermore, the devices on polymeric support are about ten times lighter compared to their rigid counterparts realized on conventional 500 µm thick Si wafers that make them cost efficient for high-volume delivery to medical institutions in, e.g., developing countries. To keep the *handling* cost of the biosensor as low as possible, we test the performance of the devices by measuring the target DNA under dry conditions after the solution is simply dripped onto the sensing area of the detector.

2. Results

2.1. Fabrication of SiNW-FET on PI Foils

A SiNW-FET with high output currents and low power dissipation is the key component of the developed diagnostic platform. Fabrication of transistor devices on a flexible support imposes certain constraints, especially on the maximum allowed processing temperature. First, we grow dense arrays of vertically aligned intrinsic Si nanowires with a mean diameter of 22 nm and length of 3–20 µm onto rigid Si wafers using the vapor–liquid–solid (VLS) growth mechanism[37–39] (see the Experimental Section). Applying the contact printing approach,[40,41] we transfer onto a receiver flexible support up to 10^3 SiNWs per device over an area of 80 µm × 400 µm (areal density of the SiNWs: 0.03 nanowires µm^{-2}). As a flexible support, we chose 100 µm thick polyimide foils (PI, Dupont HN100) owing to the exceptionally good mechanical, thermal, and chemical stability, which enables their extended use in state-of-the-art consumer electronics. After the transfer process (see the Experimental Section), the nanowires are aligned

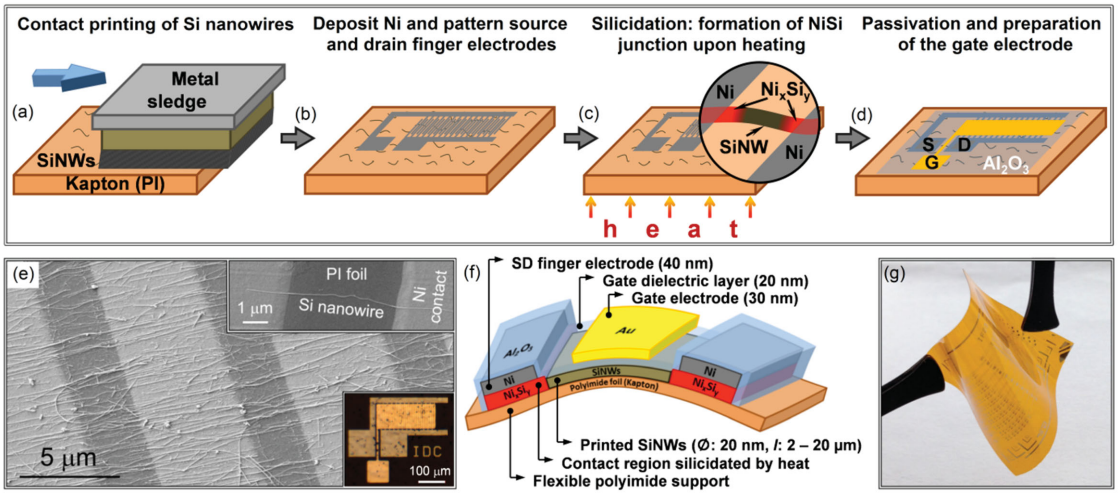

Figure 1. Schematics revealing the key fabrication steps to realize the light weight and flexible biosensing platform based on flexible SiNW-FET devices. a) Contact printing of vertically aligned SiNW onto flexible PI foils with a thickness of 100 µm. b) Deposition and patterning the source-drain electrodes. c) Silicidation process to realize NiSi junction between SiNW and Ni electrodes. d) Deposition and patterning of the gate dielectric and gate electrode. e) SEM image of the array of SiNWs bridging the finger electrodes. The top inset shows the close-up area with a single SiNW. Bottom inset: optical image of the SiNW-FET device on flexible PI foil. f) Schematics of the cross-section through the key functional layers in the device layout. g) Optical image of the resulting diagnostic platform consisting of arrays of the transistor devices that can be bent at will after fabrication.

Adv. Healthcare Mater. **2015**,
DOI: 10.1002/adhm.201500128

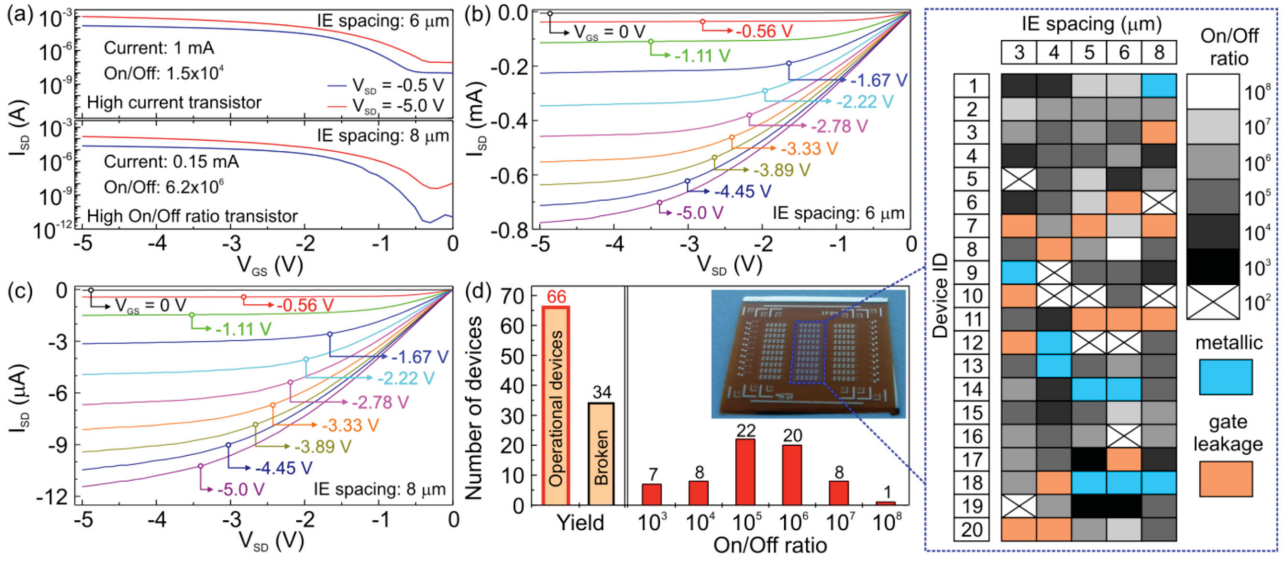

Figure 2. Electrical characterization of SiNW-FETs. a) Transfer and b,c) output characteristics of the flexible transistors with interelectrode (IE) spacing of 6 and 8 µm. d) Statistics with the number of the functional devices and their corresponding on/off ratios. The inset shows the array of the measured devices. The schematic close-up at the right-hand side contains a mapping of the device specific on/off ratios.

horizontally on the foil (Figure 1a) allowing their integration into a standard FET geometry. As a single nanowire device delivers current output of about 1 µA only,[11,39,42–44] parallel arrays of SiNWs are used in this work to deliver macroscopic current outputs.[40,41,45] Furthermore, devices with large numbers of NWs connected in parallel are characterized by a broader dynamic range as well as higher saturation and zero field currents as beneficial for the practical realization of sensing devices. Using conventional lift-off-based optical lithography and sputter deposition of a 40 nm thick Ni film, the interdigitated source-drain (SD) electrodes are formed as shown in Figure 1b. We tuned the interelectrode spacing (IE spacing) between 3 and 8 µm to assess its impact on the performance and the yield of the working devices. To decrease the contact resistance at the interface between Si and Ni (Figure 1c), a thermal annealing process was performed after deposition of the SD electrodes. Accordingly, metallic Ni silicide grows into the nanowires delivering abrupt metal to Si nano-sized Schottky junctions.[42] The transmissibility through the contacts is strongly enhanced due to the thinning the barrier, which leads to higher current densities compared to unprocessed devices.[41] The contact resistance can therefore be reduced by two orders of magnitude (see the Experimental Section) even without the need for doping. In contrast to dopant activation at high temperatures conventionally used in CMOS, annealing is carried out at moderate temperatures of 350 °C for 20 min, activating Ni diffusion into Si.[42,46–48] The temperature is still low enough to avoid the degradation of the flexible PI foils. To realize the metal-oxide-semiconductor (MOS) transistor architecture, first, we prepare a 20 nm thick Al_2O_3 layer using atomic layer deposition (ALD). Then, the gate electrode of Cr(3 nm)/Au(40 nm) is fabricated by thermal evaporation into a lithographically predefined area followed by a lift-off process. The final transistor layout is shown in Figure 1d. In a single fabrication run, we prepare 100 flexible devices to assess the fabrication yield by, e.g., measuring transfer characteristics (see the Experimental Section).

Although prepared on a flexible support, the fabricated devices operating in the accumulation mode reveal outstanding p-type transistor performance (**Figure 2**): typical on/off current ratio as high as 6×10^6, low threshold voltage of –0.2 V, maximum saturation source-drain current of typically up to 1 mA at $V_{SD} = -5$ V and $V_{SG} = -5$ V, subthreshold swing of 130 mV dec^{-1}. With these characteristics, the flexible SiNW-FET devices are comparable to or even outperform their rigid counterparts prepared by the top-down technology,[49,50] as well as previously reported SiNWs transistors on flexible PET foils.[51]

The measured transfer characteristics of the devices reveal the p-channel MOSFET behavior with rather small leakage currents (source-gate current, I_{SG}) of less than 10^{-8} A (Figure S1, Supporting Information). The p-type behavior of the initially intrinsic silicon nanowire is caused by the presence of negative charged traps in the interface oxide between Si and Al_2O_3 as shown in the capacitance–voltage (C–V) characteristics (Figure S2, Supporting Information). The trapped negative charges reduce the threshold voltage in the accumulation mode almost down to 0 V, hence enabling the low voltage operation of the devices and the possibility of operating in an electrolytic environment. This ensures that low operation potentials do not lead to breakdown or hydrolysis of the investigated media and therefore prevents damage to the devices.

The transfer process of SiNWs to flexible foils cannot guarantee a homogeneous distribution of the nanowires over large areas.[18] On the device level, this leads to the variation of the performance between the transistors fabricated in a single run mainly due to different numbers of NWs connecting source and drain. An overview over the performances of 100 flexible devices is shown in Figure 2d. Here, we consider the on/off current ratio as a criteria for comparison among transistors biased to $V_{SD} = 2$ V. The variation of the on/off current ratio of

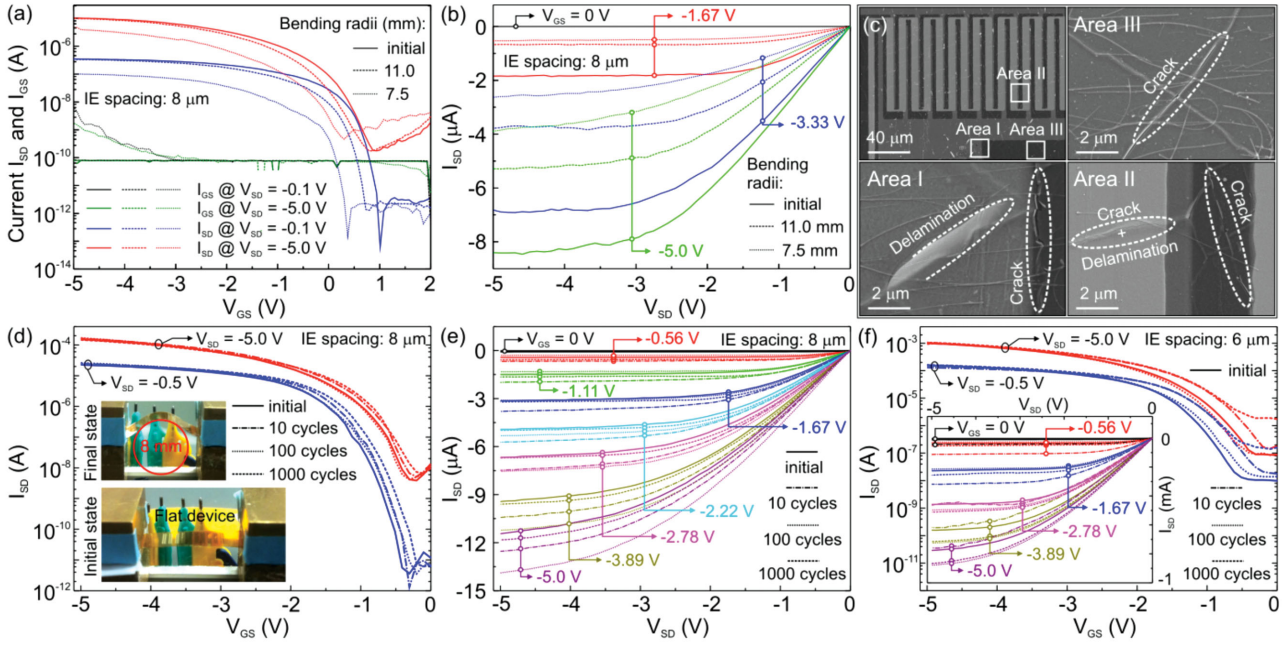

Figure 3. Mechanical performance of the flexible SiNW-FET devices. Evolution of the a) transfer and b) output characteristics of the transistors with IE spacing of 8 μm upon bending to different radii. Bending is performed in the direction parallel to SiNWs. The insets show the tested array of devices mounted into the automated bending setup (see the Experimental Section) when flat (bottom) and bent to the target radius of this experiment (top). c) SEM imaging of different areas of the device after bending to the smallest radius. The images reveal appearance of defects in the functional layers resulting in the degradation or even failure of the devices. Modification of the transfer and output characteristics of the transistors with IE spacing of d,e) 8 μm and f) 6 μm after cyclic bending to a radius of 8 mm.

the transistors in the array is color coded with the black (white) color corresponding to the lowest (highest) value, respectively. The data reveal no correlation between the device performance and the SD interelectrode spacing. Out of 100 investigated devices, 34 transistors are assigned as not operational with either high gate current leakage, or revealing metallic behavior, or possessing on/off current ratio of less than 10^2. All other 66% of the devices are operating properly with the on/off current ratio higher than 10^3. The statistics on the performance of the transistors reveals that the majority of the devices possess an average on/off ratio of 10^5–10^6 independent of the IE spacing. Therefore, for the further discussion, we focus on two representative devices with the IE spacing of 6 and 8 μm revealing distinct electrical performance (Figures 2a and S1, Supporting Information). The leakage current remains lower than 10^{-8} A independent of the IE spacing and gate voltage of up to –5 V (Figure S1, Supporting Information). At the same time, the saturation currents differ by an order of magnitude: 10^{-4} and 10^{-5} A for the transistors with IE spacing of 6 and 8 μm, respectively. The observed differences in the transistor characteristics are assigned to the distinct number of SiNWs connecting source and drain and the longer Si channel, leading to a larger channel resistance.

2.2. Mechanical Performance of SiNW-FET on PI Foils

To evaluate the mechanical performance of the flexible SiNW-FET, the devices were characterized while bending to different radii down to 7.5 mm in the direction parallel and perpendicular to the Si nanowires (**Figure 3** and Figures S3, S4, Supporting Information). These bending radii are typical for the functional elements prepared on 100 μm thick flexible foils.[52–54] Smaller bending radii can be achieved when switching to thinner flexible foils.[21,29,55] The transfer characteristics of the devices are measured before bending and each time the device is placed on cylindrically shaped adapters of different radii (Figure S3, Supporting Information). Independent of the bending direction (Figure S4, Supporting Information), the devices remain fully operational even when bent to a radius of 7.5 mm. However, impact of bending on the performance of the devices is reflected in the slight shift of the threshold voltage, change of the surface leakage current of the SiNWs, and variation of the saturation current caused by the tensile stress created in the nanowire.[56] The tensile strain on the device surface can be estimated from the ratio of total thickness to bending diameter[57] and is equal to 0.67% for a bending radius of 7.5 mm. The main reason for the device degradation for even smaller bending radii is attributed to cracking and/or delamination of the brittle isolating Al_2O_3 layer, as well as a damage of the SiNWs/Ni electrode junctions upon applying the tensile strain to the layer stack. The SEM image of the device after the bending test is shown in Figure 3c, revealing that the delamination (areas I and II) and cracking (areas I, II, and III) is taking place at various locations of the sample. In particular, a crack in the Al_2O_3 layer spanning across the array of SiNWs is clearly visible in areas II and III, which contain only the Al_2O_3 layer deposited on a PI foil. Cracks in the metal layers are observed by SEM as well (area II).

The robustness of the device against uninterrupted mechanical deformation was tested by reversibly bending the device

Adv. Healthcare Mater. 2015,
DOI: 10.1002/adhm.201500128

(see the Experimental Section) in the direction parallel to the Si nanowires to a constant target radius of 8 mm (strain: 0.62%). The cyclic bending experiments (Figure 3d–f) were carried out using another device than the one used for determining the minimum bending radii (Figure 3a,b). The output and transfer characteristics of the device are measured before and after the cycling test. Remarkably, even after 1000 cycles of bending close to the failure limit the device delivers full performance (Figure 3d–f).

2.3. Flexible Biosensor Platform

For the application of the devices as biosensors, a modified design with longer interconnects between device and contact pads was applied to avoid the contact of nonpassivated electrical leads and solvents used for chemical functionalization and biosensing assays. In order to use the flexible devices for the specific detection of AIV subtype H1N1, the chemical functionalization of the fabricated nanowire devices was realized prior to attaching the probe DNA sequences. The surface modification protocol was based on immobilization of amino-modified DNA probe sequences on hydroxylated surfaces[58] and is summarized in **Figure 4**a. First, the surface (OH) groups were activated by oxygen plasma treatment, followed by a silanization step in an ethanol solution containing 2% aminopropyltrieth-oxysilane (APTES) and 5% DI H_2O for 60 min. The resulting aminated surface was further modified by succinic anhydride to provide exposed carboxylic groups at the surface, as described in the Experimental Section. After rinsing in borate buffer, the probe oligonucleotide was immobilized (PBS buffer with a 20×10^{-6} M of DNA, incubated for 60 min). This oligonucleotide (sequence: 5′-NH_2-$(CH_2)_6$-CAC ACT CTG TCA ACC TAC-3′), which is complementary to a target DNA sequence of the H1N1 AIV (sequence: 5′-GTA GGT TGA CAG AGT GTG-3′), presents a 5′ modification with an amino group that could be bound to activated carboxilyc groups present at the active area of the sensors. The functionalized devices were rinsed again and a blocking step of the unreacted carboxylic groups in 0.5 mg mL^{-1} bovine serum albumin (BSA) was performed in Tris-HCl buffer in the presence of 20×10^{-3} M $MgCl_2$ to promote DNA folding. After a final rinse, the devices were ready to use. The functionalization process resulted in a device with a higher conductivity compared to the native state, as observed by a measurement of the output characteristic by sweeping the source-drain voltage, V_{SD}, from −2 to 2 V (Figure 4b, compare

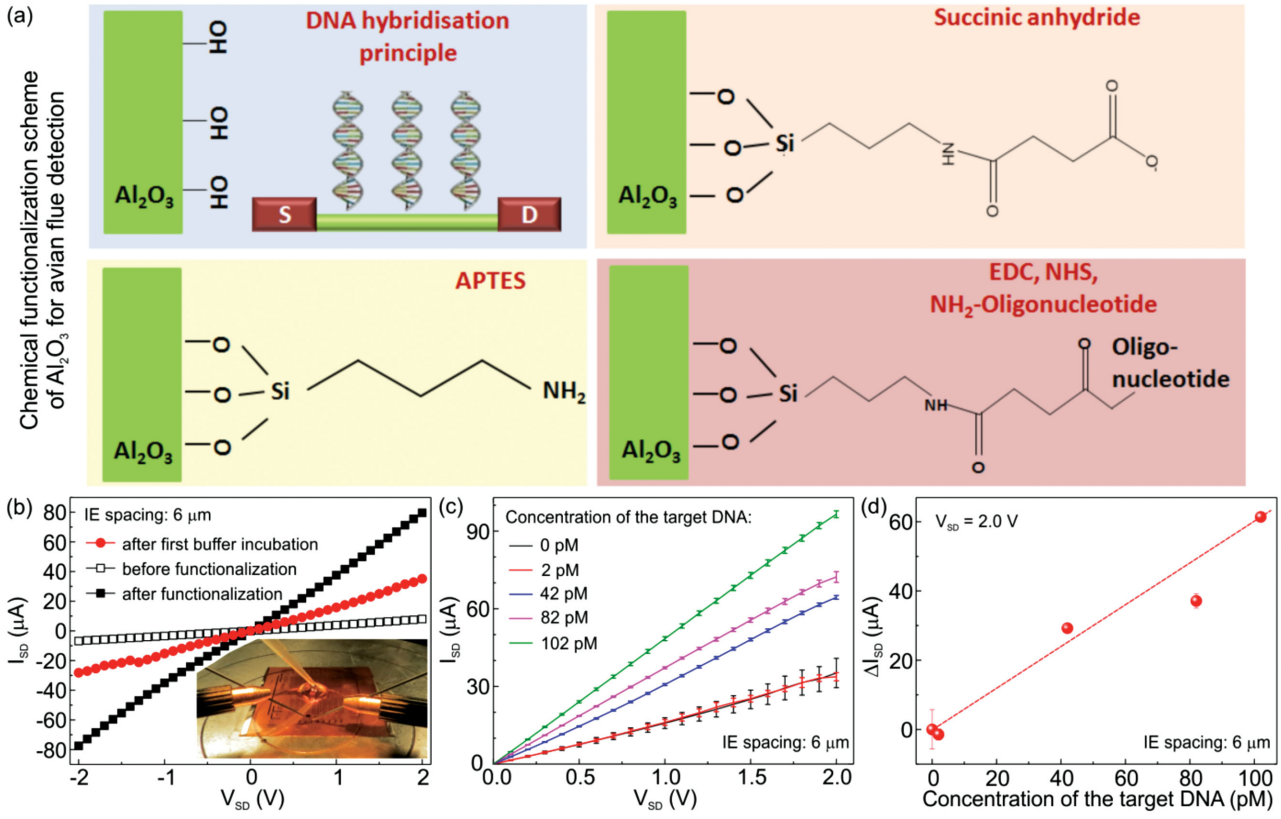

Figure 4. Use of the flexible platform to detect the Avian Influenza Virus (AIV) subtype H1N1 DNA sequences. a) Chemical functionalization scheme. b) Output characteristics of the flexible SiNW-FETs used for the DNA sensing before and after the functionalization. Measurement after the first incubation in buffer containing no target DNA is used as a reference. The inset shows measurements setup: two needles connected the electrical contact pads with the data acquisition device and a micropipette was used to deposit each DNA sample and the rinsing buffer. c) Output characteristics after the accumulation of hybridized target DNA in the picomolar range (device with IE spacing of 6 µm). Error bars represent the standard deviation of the mean value of three consecutive sweepings after each hybridization step in order to determine the repeatability of the measurements. d) Change of the source-drain current taken at V_{SD} = 2 V with the concentration of the target DNA.

data in open and closed squares). This increase is related to the presence of negatively charged phosphates in the DNA backbone structure.[59]

In order to sense the Avian Influenza Virus, the evolution of the source-drain current I_{SD} was monitored after hybridization of the DNA molecules with complementary oligonucleotides at different concentrations. A 100 µL droplet containing oligonucleotides was incubated for 30 min. After rinsing and drying in N_2, the output characteristic of the device was measured. However, a remaining thin liquid film that enables the dissolution of salt ions and their movement toward the surface[60] causes a decrease of the measured signal (Figure 4b, closed circles). Hence, the reference measurement in a buffer containing no target DNA was always taken prior to the incubation. A buffer of 10×10^{-3} M PBS was used for such a reference measurement and for the DNA hybridization. We note that the used buffer possesses low ionic concentration compared to the one used in microarray technology, which contains a six-time higher concentration of NaCl.[61] Assuring the low salt concentration is crucial to prevent the salt cluster formation and the presence of an excess of ions on the remaining thin film that could decrease the sensitivity of the device.

Consecutive incubations of the target DNA in the picomolar range caused an accumulation of hybridized strands, which can be understood as an accumulation of negative charges that induce an increase of the current values (Figure 4c).[62] In short double-stranded DNA molecules the hydrophobic nucleotide base-pairs lie within the biomolecule, while the negatively charged phosphates remain outside repelling each other, being energetically favorable to be a straight molecule[63] and allowing the electrostatic interaction with the carriers that move through the nanowire channels of the FET. To analyze the limit of detection, we monitor the changes of current values for different concentrations of the target DNA molecules at fixed SD voltage V_{SD} = 2.0 V (Figure 4d). Although small changes are observed for 2×10^{-12} M DNA, a clear increase of the current is detected already at 40×10^{-12} M.

3. Discussions

The biosensor devices on flexible foils should offer quick, easy, and cost-efficient tests, when the analyte is simply dripped onto the sensing area of the detector. In this concept, the diagnostics chips are not equipped with microfluidic channels or other reservoirs, where the shape and volume of the liquid analyte, as well as, e.g., capacitance values are well controlled. Therefore, in order to avoid the influence of the aforementioned issues on the result, the measurement of the target DNA is carried out under dry conditions. This scheme is also beneficial to eliminate the Debye screening problem that affects the measurement of liquid samples using FETs.[64] Furthermore, the measurements were performed with the thermodynamically undefined gate voltage (no gate voltage applied). This configuration is similar to the first realizations of the ion-sensitive solid-state devices.[65]

The underlying sensing mechanism is the gating effect, which is possible due to the modification of the surface potential at the nanowires, when the surface charge density changes upon molecules binding events. It has to be stressed that generally not all of ssDNA will hybridize with the probe sequences at the nanowire surface due to their electrostatic repulsion on binding sites. Typically, the hybridization probability varies in the range from 5 to 50%,[62] depending on the ionic strength of the buffer. Further reduction of the sensing efficiency can be expected due to the nonideal activation of the alumina surface. In order to determine the limit of detection and the sensitivity of the devices, the following estimates were performed. First, we calculate the sensing area of all Si nanowires per device with IE spacing of 6 µm. This area is estimated to be 165 µm^2 (= $\pi DL\eta N\sigma$) under the following assumptions:

- each nanowire of a cylindrical shape has a diameter of D = 22 nm and length of 10 µm (= averaged value based on statistical analysis in the array of nanowires with the length from 3 to 20 µm);
- working length of a nanowire for the device with IE spacing of 6 µm is L = 6 µm;
- the semiconducting length of a nanowire after the silicidation process is η = 70%;[45]
- there are approximately N = 1000 nanowires per device;
- from the total amount, only those SiNWs contribute to the sensing process, which are located between the metal electrodes. For the device with the IE spacing of 6 µm, this area is about σ = 57% of the total active Si surface of the device.

Taking the average diameter of a single ssDNA molecule to be 2 nm and assuming the separation between neighboring molecules of 2 nm, the surface area occupied by a molecule is $[\pi \times (4\ \text{nm}/2)^2] = 12.56\ \text{nm}^2$. Hence, there will be 1.3×10^7 surface states available for the detection of the molecules. If we want to detect 100×10^{-12} M of the ssDNA, this corresponds to 6.02×10^9 molecules in 100 µL of the sample solution. Out of 6.02×10^9 molecules, only the fraction settled at the working area occupied by the SiNWs will contribute to the detected signal. This fraction can be estimated by the ratio of the area occupied by the active area of the nanowires to the total area of the droplet [165 µm^2/28 mm^2] = 5.9×10^{-6} multiplied on the total number of molecules, resulting in the total number of molecules to be detected N_0 = [6.02×10^9 molecules × 5.9×10^{-6}] = 3.6×10^4. As the number of the available surface states (1.3×10^7 states) is substantially larger than the total number of molecules to be detected, the device is working well before its active surface is saturated. Furthermore, we note that the total surface occupied by the molecules is [12.56 nm^2/molecule × 6.02×10^9 molecules] = 75.6×10^3 µm^2. This is substantially smaller than the area of the droplet of 28 mm^2 initially spread over the device. In this respect, the homogeneous coverage of the device area by the ssDNA molecules is expected.

Capacitance of the device can be roughly estimated as $C = \varepsilon\varepsilon_0 S/d$, with $\varepsilon_0 = 8.85 \times 10^{-12}$ F m^{-1}. We use d = 20 nm thick Al_2O_3 gate dielectric with the electric permittivity of ε = 2.5. Accounting for the active surface area, S, of the SiNWs of 165 µm^2 contributing to the sensing process, we obtain that C = 182 fF.

To minimize the impact onto the depletion layer of SiNWs, V_{SD} should be chosen as small as possible in the range of several mV. Therefore, while calculating the electrical charge based

DOI: 10.1002/adhm.201500128

on the known capacitance of the device, we have to consider the threshold voltage only. By interpolation to $I_{SD} = 0$ A in the linear scale of I_{SD} versus V_{GS}, the threshold voltage is $V_{TH} = -1.5$ V (Figure 3f). The total charge is $q = C \times V_{TH} = -273$ fC. To calculate the number of the ssDNA molecules, N_C, that are needed to open the transistor, we note that each of the ssDNA molecules carries 18 negative electrical charges and we should take into account doubling of the surface charge due the interaction between DNA molecules and functionalized layer (DNA-DNA hybridization). Hence, $N_C = q/[2 \times 18 \times q_0] = 4.7 \times 10^4$. In our case, the number of available molecules for detection is $N_0 = 3.6 \times 10^4$ that means that the transistor is working in the subthreshold regime. The latter is crucial to assure its high sensitivity. When detecting 3.6×10^4 molecules, the voltage induced by them is $V = 2 \times 18 \times N_0 \times q_0/C = -1.14$ V leading to the subthreshold current of about 60 µA. In this respect, the data presented in the inset in Figure 3f are in *quantitative* agreement with the biosensing results in Figure 4c. The limit of detection, N_{DL}, of the device is defined by the "cut-off" voltage of –0.48 V (Figure 3f, red curve), which corresponds to $N_{DL} = 1.5 \times 10^4$ molecules. With this limit of detection, the device is able to measure about 40×10^{-12} M of the ssDNA molecules as observed experimentally (Figure 4c,d). Remarkably, the flexible biosensing platform is comparable in the detection performance with the rigid counterparts.[66,67] The detection limit of the flexible diagnostic platform could be potentially enhanced by reduction of the "cut-off" and threshold voltages. This can be achieved through the surface treatment in order to compensate for positive surface charges.

Using the flexible SiNW-FETs, the influenza virus is successfully detected within about 30 min only including the incubation and measurement time. The fast detection ability of our analytic platform suggests its suitability for an early-stage disease diagnostic. This performance is superior compared to standard methods such as viral culture, which takes up to 14 d for the diagnosis of influenza whose duration is 5–7 d.[68] In addition, our detection platform minimizes the risk of false positives that could occur in fast and highly sensitive methods such as PCR. Indeed, the PCR requires about half an hour for the detection of a single molecule through its amplification into more copies, but at the same time a contaminant DNA molecule could also be amplified leading to its detection.[69,70]

4. Conclusion

We put forth an approach to fabricate a lightweight and flexible diagnostic platform for early detection of the Avian Influenza Virus (AIV) subtype H1N1 DNA sequences. The biosensing is realized based on the high-performance Si nanowire field effect transistors, which are optimized on extended 100 µm thick polyimide foils. The devices withstand severe mechanical deformations, namely, they can be bent down to 7.5 mm radius and retain their performance after 1000 bending cycles. In addition to its appealing mechanical properties, the device reveals remarkable analytic performance with the limit of detection of the target DNA molecules of 40×10^{-12} M and the detection time of 30 min only. This is achieved without use of microfluidic channels or other reservoirs by simply dripping the solution with the analyte onto the sensing area of the detector and measuring under dry conditions. The main motivation for the applied measurement scheme is to keep the handling cost of the biosensor as low as possible.

The devices on a polymeric support possess unique features: they are about ten times lighter compared to their rigid counterparts realized on Si wafers and can be prepared on large areas. This results in the reduction of the price per device and makes them cost efficient for high-volume delivery to medical institutions in, e.g., developing countries. We envision that the realization of the sensitive diagnostic platform, which can be fabricated on cost-efficient large area flexible foils by roll-to-roll methods, will allow the timely diagnosis of the viral or infectious diseases, e.g., the here demonstrated H1N1 subtype of the AIV, in the developing countries. The early detection of this and other harmful virus species is absolutely crucial as a prevention mechanism for its epidemic spreading.

5. Experimental Section

Fabrication of the Si Nanowires: Silicon nanowires were grown in a CVD furnace (ATV technology GmbH) with Au seed particles of 20 nm mean diameter (GNPs, Plano GmbH). Au particle decorate the SiO_2 coated Si growth wafers (up to 8 in., p-doped boron 116 cm^3) were exposed to SiH_4/H_2 (1/10 p/p) gas mixture at a pressure of 65 mbar at 400 °C for 40 min. Growth rate of nominally undoped Si nanowires was approximately 1 µm min^{-1} for the chosen recipe.[41]

Transfer of SiNWs to the PI Foils: A contact printing method was applied to transfer arrays of SiNWs (length: 3–20 µm, diameter: 22 nm) onto flexible Polyimide foils. The donor Si wafer with a dense array of SiNWs was attached onto a metal sledge to make a directional sliding on top of the receiver flexible foil. The sledge was pushed to the predetermined path and the van der Waals interaction induced the detachment of the SiNWs from the donor substrate to the receiver substrate.

Silicidation Process: A thermal annealing process was followed after the deposition of the SD electrodes to create a metal silicide. The thermally activated axial intrusion of Ni_xSi_y from the Ni electrodes to the SiNWs was performed in a high temperature annealing chamber in the forming gas N_2/H_2 (10/1 p/p) atmosphere. The vacuum in the chamber was kept at 0.06 bar during processing. The thermal annealing was carried out at 350 °C for 20 min to form the $NiSi_2$ phase and to avoid the deformation of the PI film by heating. To evaluate the influence of the silicidation process at the device performance, electrical characteristics of the devices were measured before and after the thermal annealing process (Figure S5, Supporting Information). SD currents through the SD voltage swing from –2 to 2 V were measured using a Keithley source meter. The SD current was increased approximately by the factor of 100 after the thermal annealing process. A bright color, which was typical of the nickel silicide, was not observed by the SEM investigation. It was suggest that only a small part of the SiNWs underneath the Ni electrode was silicidized owing to the relatively low processing temperature. The annealing process period was extended from 20 to 60 min to increase the diffusion of the Ni electrode to the SiNWs. Contrary to the expectation, no phase of the Ni_xSi_y was observed by SEM. Instead of the diffused Ni_xSi_y, traces of Si were observed at the edges of the SiNWs. This might occur due to the different thermal expansions of the PI film and SiNWs. According to the data sheet of the PI film, approximately 1.3% of residual shrinkage took place at the 400 °C temperature. Since the SiNWs had higher thermal stability compared to the PI film, traces of SiNWs might be formed by partial delamination and sliding on the PI support during the expansion and contraction. Therefore, prolonged thermal annealing processes should be avoided.

Analysis of the Total Yield of the Working Devices: In a single fabrication run, transfer characteristics of 100 flexible devices were prepared and

measured to assess the fabrication yield. The 34 elements, which were defined as bad working devices, either had high gate current leakages or had an on/off current ratio of less than 10^2. These poorly working devices did not occur at one particular place, but were scattered throughout the array. It was assumed that the main reason of the device failure was due to the accumulation of, e.g., dust particles or other inclusions onto the surfaces of either the flexible foil or the functional elements of the transistor during the fabrication process (Figure S6, Supporting Information).

Bending Setup: The bending experiments were realized on a motor-controlled mechanical loading setup. The sample was mounted on a loading stage, one end of which was precisely driven by a motor to move with a speed of 100 µm s^{-1} over a defined distance while the other end was fixed.

Biofunctionalization Process: First, the surface (OH) groups were activated by oxygen plasma treatment, followed by a silanization step in an ethanol solution containing 2% aminopropyltriethoxysilane (APTES) and 5% DI H_2O for 1 h. After rinsing the devices with ethanol to remove the nonspecifically bound APTES molecules, a postbake at 110 °C for 30 min was carried out, resulting in amino groups at the surface. These were further modified into carboxylic groups by an incubation for 60 min in a succinic anhydride dissolved in dimethyl sulfoxide (DMSO) and diluted in 200×10^{-3} M borate buffer pH 8 (with a final concentration of 10 mg mL^{-1}). Here, the ring structure of the molecule opened, leaving an exposed carboxylic group. After rinsing in borate buffer, an incubation for 10 min in a 10×10^{-3} M 1-ethyl-3-(3-dimethylaminopropyl)-carbodiimide (EDC) and 5×10^{-3} M *N*-hydroxysuccinimide (NHS) solution in phosphate buffered saline (PBS) buffer pH 7.4 was carried out in order to activate the carboxylic groups. Then, the amino-modified probe oligonucleotide was immobilized (20×10^{-6} M of DNA in PBS) by incubation for 1 h. The functionalized devices were rinsed again and the unreacted carboxylic groups were blocked by an incubation for 30 min in 0.5 mg mL^{-1} BSA in Tris-HCl buffer. This buffer contained 20×10^{-3} M $MgCl_2$ to promote DNA folding. A final rinse left the devices ready to use.

Supporting Information

Supporting Information is available from the Wiley Online Library or from the author.

Acknowledgements

D.K. and B.I. contributed equally to this work. The authors thank Mrs. C. Krien (IFW Dresden) for assistance in deposition of thin metal films, A. Kutscher (IFW Dresden) for support in investigation of the bending performance of the transistors, and Dr. M. Brehm (IFW Dresden) for help in SiO_2 etching. The support in the development of the experimental setups from the Research Technology Department of the IFW Dresden and the clean room maintenance by Dr. S. Harazim (IFW Dresden) is greatly appreciated. This work was financed in part via the European Research Council within the European Union's Seventh Framework Programme (FP7/2007-2013)/ERC Grant Agreement No. 306277. Furthermore, the authors acknowledge support from the German Excellence Initiative via the Cluster of Excellence EXC 1056 "Center for Advancing Electronics Dresden" (cfAED).

Received: February 24, 2015
Revised: April 13, 2015
Published online:

[1] G. Zheng, F. Patolsky, Y. Cui, W. U. Wang, C. M. Lieber, *Nat. Biotechnol.* **2005**, *23*, 1294.
[2] A. S. Dighe, K. Lewandrowski, *Point Care* **2005**, *4*, 86.
[3] S. S. Ehrmeyer, R. H. Laessig, *Clin. Chem. Lab. Med.* **2007**, *45*, 766.
[4] Y. H. Lao, K. Peck, L. C. Chen, *Anal. Chem.* **2009**, *81*, 1747.
[5] A. Gao, N. Lu, P. Dai, T. Li, H. Pei, X. Gao, Y. Gong, Y. Wang, C. Fan, *Nano Lett.* **2011**, *11*, 3974.
[6] T. Kurkina, A. Vlandas, A. Ahmad, D. Kern, K. Balasubramanian, *Angew. Chem. Int. Ed.* **2011**, *50*, 3710.
[7] A. Niemz, T. M. Ferguson, D. S. Boyle, *Trends Biotechnol.* **2011**, *29*, 240.
[8] http://www.who.int/influenzavaccinesplan/resources/progress_materials/en/(accessed: April **2015**).
[9] J. T. Wu, S. Riley, C. Fraser, G. M. Leung, *PLoS Med.* **2006**, *3*, e361.
[10] Y. Cui, Q. Wei, H. Park, C. M. Lieber, *Science* **2001**, *293*, 1289.
[11] A. Heinzig, S. Slesazeck, F. Kreupl, T. Mikolajick, W. M Weber, *Nano Lett.* **2011**, *12*, 119.
[12] A. Tarasov, M. Wipf, K. Bedner, J. Kurz, W. Fu, V. A. Guzenko, O. Knopfmacher, R. L. Stoop, M. Calame, C. Schönenberger, *Langmuir* **2012**, *28*, 9899.
[13] F. Patolsky, G. Zheng, O. Hayden, M. Lakadamyali, X. Zhuang, C. M. Lieber, *Proc. Natl. Acad. Sci. U.S.A.* **2004**, *101*, 14017.
[14] J. Wang, F. Shen, Z. Wang, G. He, J. Qin, N. Cheng, M. Yao, L. Li, X. Guo, *Angew. Chem. Int. Ed.* **2014**, *53*, 1.
[15] D. E. Bidwell, A. Bartlett, A. Voller, *J. Infect. Dis.* **1977**, *136*, S274.
[16] A. D. Ellington, J. W. Szostak, *Nature* **1990**, *346*, 818.
[17] J. A. Streifer, H. Kim, B. M. Nichols, R. J. Hamers, *Nanotechnology* **2005**, *16*, 1868.
[18] K. I. Chen, B. R. Li, Y. T. Chen, *Nano Today* **2011**, *6*, 131.
[19] C. D. Chin, S. Y. Chin, T. Laksanasopin, S. K. Sia, in *Point-of-Care Diagnostics on a Chip* (Eds: D. Issadore, R. M. Westervelt), Springer, New York **2013**, Ch. 1.
[20] M. Kaltenbrunner, M. S. White, E. D. Głowacki, T. Sekitani, T. Someya, N. S. Sariciftci, S. Bauer, *Nat. Commun.* **2012**, *3*, 770.
[21] M. Kaltenbrunner, T. Sekitani, J. Reeder, T. Yokota, K. Kuribara, T. Tokuhara, M. Drack, R. Schwodiauer, I. Graz, S. Bauer-Gogonea, S. Bauer, T. Someya, *Nature* **2013**, *499*, 458.
[22] A. C. Glavan, R. V. Martinez, E. J. Maxwell, A. B. Subramaniam, R. M. D. Nunes, S. Soh, G. M. Whitesides, *Lab Chip* **2013**, *13*, 2922.
[23] S. Y. Xing, J. Jiang, T. R. Pan, *Lab Chip* **2013**, *13*, 1937.
[24] P. Arenkov, A. Kukhtin, A. Gemmell, S. Voloshchuk, V. Chupeeva, A. Mirzabekov, *Anal. Biochem.* **2000**, *278*, 123.
[25] G. Lin, D. Makarov, M. Melzer, W. Si, C. Yan, O. G. Schmidt, *Lab Chip* **2014**, *14*, 4050.
[26] D.-H. Kim, J. Viventi, J. J. Amsden, J. Xiao, L. Vigeland, Y.-S. Kim, J. A. Blanco, B. Panilaitis, E. S. Frechette, D. Contreras, D. L. Kaplan, F. G. Omenetto, Y. Huang, K.-C. Hwang, M. R. Zakin, B. Litt, J. A. Rogers, *Nat. Mater.* **2010**, *9*, 511.
[27] D.-H. Kim, R. Ghaffari, N. Lu, S. Wang, S. P. Lee, H. Keum, R. D'Angelo, L. Klinker, Y. Su, C. Lu, Y.-S. Kim, A. Ameen, Y. Li, Y. Zhang, B. de Graff, Y.-Y. Hsu, Z. J. Liu, J. Ruskin, L. Xu, C. Lu, F. G. Omenetto, Y. Huang, M. Mansour, M. J. Slepian, J. A. Rogers, *Proc. Natl. Acad. Sci. U.S.A* **2012**, *109*, 19910.
[28] D. H. Kim, N. S. Lu, R. Ma, Y. S. Kim, R. H. Kim, S. D. Wang, J. Wu, S. M. Won, H. Tao, A. Islam, K. J. Yu, T. I. Kim, R. Chowdhury, M. Ying, L. Z. Xu, M. Li, H. J. Chung, H. Keum, M. McCormick, P. Liu, Y. W. Zhang, F. G. Omenetto, Y. G. Huang, T. Coleman, J. A. Rogers, *Science* **2011**, *333*, 838.
[29] M. Melzer, M. Kaltenbrunner, D. Makarov, D. Karnaushenko, D. Karnaushenko, T. Sekitani, T. Someya, O. G. Schmidt, *Nat. Commun.* **2015**, *6*, 6080.
[30] R. C. Webb, A. P. Bonifas, A. Behnaz, Y. H. Zhang, K. J. Yu, H. Y. Cheng, M. X. Shi, Z. G. Bian, Z. J. Liu, Y. S. Kim, W. H. Yeo, J. S. Park, J. Z. Song, Y. H. Li, Y. G. Huang, A. M. Gorbach, J. A. Rogers, *Nat. Mater.* **2013**, *12*, 938.
[31] M. Melzer, D. Makarov, A. Calvimontes, D. Karnaushenko, S. Baunack, R. Kaltofen, Y. F. Mei, O. G. Schmidt, *Nano Lett.* **2011**, *11*, 2522.

[32] M. Melzer, G. G. Lin, D. Makarov, O. G. Schmidt, *Adv. Mater.* **2012**, *24*, 6468.
[33] M. Melzer, M. Melzer, D. Karnaushenko, G. Lin, S. Baunack, D. Makarov, O. G. Schmidt, *Adv. Mater.* **2015**, *27*, 1333.
[34] G. Kettlgruber, M. Kaltenbrunner, C. M. Siket, R. Moser, I. M. Graz, R. Schwödiauer, S. Bauer, *J. Mater. Chem. A* **2013**, *1*, 5505.
[35] S. Xu, Y. H. Zhang, J. Cho, J. Lee, X. Huang, L. Jia, J. A. Fan, Y. W. Su, J. Su, H. G. Zhang, H. Y. Cheng, B. W. Lu, C. J. Yu, C. Chuang, T. I. Kim, T. Song, K. Shigeta, S. Kang, C. Dagdeviren, I. Petrov, P. V. Braun, Y. G. Huang, U. Paik, J. A. Rogers, *Nat. Commun.* **2013**, *4*, 1543.
[36] Y. Liu, L. Zhang, Y. Zhou, *J. Gene Ther.* **2014**, *2*, 4.
[37] R. S. Wagner, W. C. Ellis, *Appl. Phys. Lett.* **1964**, *4*, 89.
[38] Y. Wu, Y. Cui, L. Huynh, C. J. Barrelet, D. C. Bell, C. M. Lieber, *Nano Lett.* **2004**, *4*, 3.
[39] W. M. Weber, G. S. Duesberg, A. P. Graham, M. Liebau, E. Unger, C. Chèze, L. Geelhaar, P. Lugli, H. Riechert, F. Kreupl, *Phys. Status Solidi (b)* **2006**, *243*, 3340.
[40] Z. Fan, J. C. Ho, Z. A. Jacobson, R. Yerushalmi, R. L. Alley, H. Razavi, A. Javey, *Nano Lett.* **2008**, *8*, 20.
[41] S. Pregl, W. M. Weber, D. Nozaki, J. Kunstmann, L. Baraban, J. Opitz, T. Mikolajick, G. Cuniberti, *Nano Res.* **2013**, *6*, 381.
[42] W. M. Weber, L. Geelhaar, A. P. Graham, E. Unger, G. S. Duesberg, M. Liebau, W. Pamler, C. Chèze, H. Riechert, P. Lugli, F. Kreupl, *Nano Lett.* **2006**, *6*, 2660.
[43] W. M Weber, L. Geelhaar, E. Unger, C. Chèze, F. Kreupl, H. Riechert, P. Lugli, *Phys. Status Solidi (b)* **2007**, *244*, 4170.
[44] Z. Fahem, G. Csaba, C. M. Erlen, P. Lugli, W. M. Weber, L. Geelhaar, H. Riechert, *Phys. Status Solidi (c)* **2008**, *5*, 27.
[45] F. Zörgiebel, S. Pregl, L. Römhildt, J. Opitz, W. Weber, T. Mikolajick, L. Baraban, G. Cuniberti, *Nano Res.* **2014**, *7*, 267.
[46] K. N. Tu, *Annu. Rev. Mater. Sci.* **1985**, *15*, 147.
[47] B. A. Julies, D. Knoesen, R. Pretorius, D. Adams, *Thin Solid Films* **1999**, *347*, 201.
[48] F. Léonard, A. A. Talin, *Nat. Nanotechnol.* **2011**, *6*, 773.
[49] G. Wenga, E. Jacques, A. C. Salaün, R. Rogel, L. Pichon, F. Geneste, *Biosens. Bioelectron.* **2013**, *40*, 141.
[50] M. Wipf, R. L. Stoop, A. Tarasov, K. Bedner, W. Fu, I. A. Wright, C. J. Martin, E. C. Constable, M. Calame, C. Schönenberger, *ACS Nano* **2013**, *7*, 5978.
[51] M. C. McAlpine, H. Ahmad, D. Wang, J. R. Heath, *Nat. Mater.* **2007**, *6*, 379.
[52] C. Zysset, N. Münzenrieder, L. Petti, L. Büthe, G. A. Salvatore, G. Tröster, *IEEE Electron Device Lett.* **2013**, *34*, 1394.
[53] D. Karnaushenko, D. Makarov, M. Stöber, D. D. Karnaushenko, S. Baunack, O. G. Schmidt, *Adv. Mater.* **2015**, *27*, 880.
[54] M. Melzer, J. I. Mönch, D. Makarov, Y. Zabila, G. S. Canon Bermudez, D. Karnaushenko, S. Baunack, F. Bahr, C. Yan, M. Kaltenbrunner, O. G. Schmidt, *Adv. Mater.* **2015**, *27*, 1274.
[55] G. A. Salvatore, N. Münzenrieder, T. Kinkeldei, L. Petti, C. Zysset, I. Strebel, L. Büthe, G. Tröster, *Nat. Commun.* **2014**, *5*, 2982.
[56] A. Heinzig, T. Mikolajick, J. Trommer, D. Grimm, W. M. Weber, *Nano Lett.* **2013**, *13*, 4176.
[57] Z. Suo, E. Y. Ma, H. Gleskova, S. Wagner, *Appl. Phys. Lett.* **1999**, *74*, 1177.
[58] L. Römhildt, C. Pahlke, F. Zörgiebel, H. G. Braun, J. Opitz, L. Baraban, G. Cuniberti, *ACS Appl. Mater. Int.* **2013**, *5*, 12029.
[59] J. D. Watson, F. H. C. Crick, *Nature* **1953**, *171*, 737.
[60] F. Puppo, M. Di Ventra, G. De Micheli, S. Carrara, *Surf. Sci.* **2014**, *624*, 76.
[61] J. Peplies, C. Lachmund, F. O. Glöckner, W. Manz, *Appl. Environ. Microbiol.* **2006**, *72*, 4829.
[62] J. Fritz, E. B. Cooper, S. Gaudet, P. K. Sorger, S. R. Manalis, *Proc. Natl. Acad. Sci. U.S.A.* **2002**, *99*, 14142.
[63] D. J. Bakewell, N. Vergara-Irigaray, D. Holmes, *JSM Nanotechnol. Nanomed.* **2013**, *1*, 1003.
[64] F. Puppo, M. A. Doucey, T. S. Y. Moh, G. Pandraud, P. M. Sarro, G. De Micheli, S. Carrara, *Proc. IEEE Sensors Conference* **2013**, 1–4, DOI:10.1109/ICSENS.2013.6688205.
[65] P. Bergveld, *IEEE Trans. Biomed. Eng.* **1970**, *BM-17*, 70.
[66] V. C. Martins, F. A. Cardoso, P. P. Freitas, L. P. Fonseca, *J. Nanosci. Nanotechnol.* **2010**, *10*, 5994.
[67] Y. C. Li, C. C. Chiou, J. D. Luo, W. J. Chen, L. C. Su, Y. F. Chang, Y. S. Chang, C. S. Lai, C. C. Lee, C. Chou, *Biosens. Bioelectron.* **2012**, *35*, 342.
[68] K. A. Covalciuc, K. H. Webb, C. A. Carlson, *J. Clin. Microbiol.* **1999**, *37*, 3971.
[69] G. A. Storch, *Curr. Opin. Pediatr.* **2003**, *15*, 77.
[70] T. Curran, C. McCaughey, J. Ellis, S. J. Mitchell, S. A. Feeney, A. P. Watt, F. Mitchell, D. Fairley, L. Crawford, J. McKenna, P. V. Coyle, *J. Med. Microbiol.* **2012**, *61*, 332.